Impedance spectroscopy of bilayer membranes on single crystal silicon

Janice Lin, Mikhail Merzlyakov, Kalina Hristova,[a] and Peter C. Searson[a]
Department of Materials Science and Engineering, Johns Hopkins University, Baltimore, Maryland 21218

(Received 30 January 2008; accepted 21 February 2008; published 30 April 2008)

Bilayer membranes on solid supports are being developed as electrically addressable, robust, surface-supported membrane mimetics. These platforms are being explored for basic ion channel research as well as for detection and analyte sensing. The formation of bilayer membranes on semiconductor surfaces is an important step in device integration for transistor and sensor arrays. Here, the authors review the contributions to the impedance response of bilayer membranes on semiconductors, and highlight the important issues for experimental measurements. The authors also present experimental results for diphytanoyl phosphocholine bilayers formed on moderately doped and highly doped *n*-type silicon using Langmuir-Blodgett-based deposition techniques. The authors demonstrate that a detailed understanding of the contributions to the impedance response is important in developing silicon-based membrane platforms. The authors further report on the bias dependence of the impedance, and show that on highly doped *n*-type silicon, the membrane impedance can be measured over a 2 V range. © *2008 American Vacuum Society.*
[DOI: 10.1116/1.2896117]

I. INTRODUCTION

Surface-supported bilayer membranes are being developed as platforms for fundamental biophysical studies of lipids and membrane proteins, as well as for high throughput sensing.[1] Various approaches have been adopted to produce surface supported bilayers. In one approach some or all of the lipids composing the lower leaflet are tethered to the solid support, usually exploiting gold/thiol chemistry.[2–6] An alkane chain or polyethylene glycol chain attached to the head group of the lipid is conjugated with a terminal sulfhydryl group to tether the lipid to the gold support. In this case the lower leaflet is formed by self-assembly from a solution containing a mixture of lipids with and without a tether. The upper leaflet is usually formed by vesicle fusion, in which vesicles break and fuse with the lower leaflet to complete the bilayer.

An alternative approach is to use Langmuir-Blodgett (LB) deposition to transfer the lower leaflet from a compressed monolayer at the air/water interface onto the solid support.[7,8] The monolayer usually includes a fraction of lipids that have a polyethylene glycol (PEG) chain attached to the head group, which prevents direct contact between the bilayer and the solid support. In some cases, the PEG may also have a terminal group that can chemisorb to the solid support. The upper leaflet may be formed by vesicle fusion or Langmuir-Schaefer (LS). An advantage of this approach is that peptides with controlled orientation and directionality can be incorporated into the membrane in the first step.

A key feature of these methods is that the bilayer is not in direct contact with the solid support. The tether or polymer cushion provides a spacer layer or water reservoir that allows for incorporation of membrane proteins. In addition, if the fraction of lipid tethers or PEG lipids is sufficiently low, then the mobility of the lipids in the lower leaflet can mimic physiological conditions.[7] Without the polymer spacer layer, direct contact between the lipids in the lower leaflet and the support results in very low or no lipid mobility. This may increase the membrane resistance, but is not useful in creating biomimetic membranes.

In fabricating robust membrane platforms for biosensing applications, the goal is to measure a signal associated with the transport of charged species through ion channels. Two methods are commonly used for signal transduction: impedance spectroscopy and current measurements. In the absence of faradaic reactions that can occur at the support electrode, the transport of ionic species through a channel is usually detected by measuring the impedance response.[9,10] If the species transported through the channel is electroactive, then a dc current flow can be measured at the support electrode as long as there is a thermodynamic driving force for the reaction to occur.

In this paper we report on the impedance response of bilayers on single crystal silicon. The formation of bilayer membranes on silicon is the first step toward developing membrane transistor and sensor arrays for electrical or electro-optical detection.[11–14]

II. IMPEDANCE SPECTROSCOPY OF SUPPORTED BILAYER MEMBRANES

In this section we provide an overview of the impedance response of supported bilayer membranes and identify the conditions that allow measurement of ion channel conductance on semiconductors. Figure 1 shows the equivalent circuit for a supported bilayer membrane with a polymer cushion on a solid support. The series resistance R_s represents the uncompensated resistances in the circuit and includes the solution resistance and the resistances associated with the leads and contacts. For a uniform bilayer membrane without ion channels, the impedance of the bilayer can be represented by

[a]Authors to whom correspondence should be addressed; electronic mail: kh@jhu.edu; searson@jhu.edu

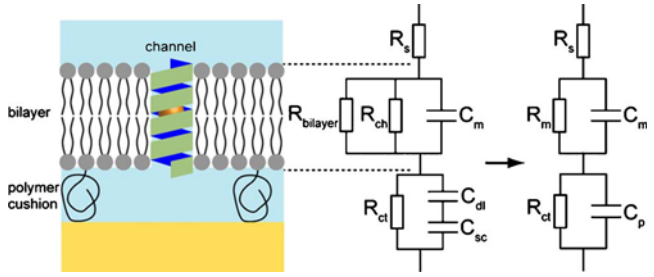

FIG. 1. Equivalent circuit for bilayer membranes on a semiconductor support. R_s: series resistance; R_m: membrane resistance ($1/R_m = 1/R_{\text{bilayer}} + 1/R_{\text{ch}}$, where R_{bilayer} is the resistance of the lipid bilayer and R_{ch} is the resistance of any ion channels); C_m: membrane capacitance; R_{ct}: charge transfer resistance at the semiconductor/solution interface; C_p: parallel capacitance (space charge layer capacitance C_{sc} or electrochemical double layer capacitance C_{dl}).

a parallel resistance and capacitance, R_{bilayer} and C_m, respectively. The capacitance can usually be considered as a parallel plate capacitor with $C = \varepsilon\varepsilon_0/d$, where ε is the relative permittivity, ε_0 is the permittivity of free space, and d is the membrane thickness. Both capacitance and resistance are normalized to the area of the support, so that C has units of F cm^{-2} and R has units of Ω cm^2. The membrane resistance, R_m, contains the resistance of the lipid bilayer, R_{bilayer}, in parallel with the resistance associated with any channels in the membrane, R_{ch}. These resistances are related by

$$\frac{1}{R_m} = \frac{1}{R_{\text{bilayer}}} + \frac{1}{R_{\text{ch}}}, \tag{1}$$

and hence

$$R_m = \frac{R_{\text{bilayer}} R_{\text{ch}}}{R_{\text{bilayer}} + R_{\text{ch}}}. \tag{2}$$

From Eq. (2) we can see that if $R_{\text{ch}} < R_{\text{bilayer}}$, then $R_m \approx R_{\text{ch}}$. Thus, the resistance associated with the channels can be extracted from the measured impedance as long as R_{ch} is less than R_{bilayer}. Also note that the membrane admittance $Y_m = n_{\text{ch}} g_{\text{ch}}$, where n_{ch} is the channel density (cm^{-2}) and g_{ch} is the channel conductance (S). Thus, in the absence of channels $R_m = R_{\text{bilayer}}$ and should be as large as possible to maximize the dynamic range.

In series with the impedance associated with the membrane is the impedance associated with the electrochemical interface. This impedance includes a charge transfer resistance, R_{ct}, associated with electron transfer across the interface. This resistance is in parallel with a capacitance C_p that includes the double layer capacitance C_{dl} and the capacitance associated with the semiconductor space charge layer C_{sc}.

The total parallel capacitance C_p associated with the electrochemical interface is given by

$$C_p = \frac{C_{\text{dl}} C_{\text{sc}}}{C_{\text{dl}} + C_{\text{sc}}}. \tag{3}$$

Hence, $C_p \approx C_{\text{sc}}$ if $C_{\text{sc}} < C_{\text{dl}}$; otherwise $C_p \approx C_{\text{dl}}$ if $C_{\text{dl}} < C_{\text{sc}}$.

The total impedance of the equivalent circuit shown in Fig. 1 is given by

$$Z(\omega) = \left(R_s + \frac{R_m}{1 + \omega^2 C_m^2 R_m^2} + \frac{R_{\text{ct}}}{1 + \omega^2 C_p^2 R_{\text{ct}}^2} \right) - i\left(\frac{\omega C_m R_m^2}{1 + \omega^2 C_m^2 R_m^2} + \frac{\omega C_p R_{\text{ct}}^2}{1 + \omega^2 C_p^2 R_{\text{ct}}^2} \right), \tag{4}$$

where the first term in parentheses is the real part of the impedance Z_{real}, and the second term in parentheses is the imaginary part of the impedance, Z_{imag}.

The magnitude of the impedance is given by

$$|Z| = \sqrt{Z_{\text{real}}^2 + Z_{\text{imag}}^2}. \tag{5}$$

The phase angle, θ, is given by

$$\theta = \tan^{-1}(Z_{\text{imag}}/Z_{\text{real}}). \tag{6}$$

For an artificial bilayer to be a good model system, it should have values of resistance and capacitance that are seen in cell membranes. The capacitance of a lipid bilayer can be estimated from the parallel plate capacitor model ($C = \varepsilon\varepsilon_0/d$). Taking a typical hydrophobic thickness of about 4 nm and a relative permittivity of 2–4, the membrane capacitance is expected to be 0.5–1 μF cm^{-2}. Values in this range have been reported experimentally.[10,12–14]

Typical values of transmembrane resistance are in the range 10^4–10^7 Ω cm^2. The normalized impedance can be compared to black lipid membrane or patch clamp experiments by considering the area of the orifice over which the membrane is suspended. A 100 GΩ seal over an orifice with a radius of 5 μm would be about 8×10^4 Ω cm^2. The time constant (in seconds) associated with relaxations at a bilayer membrane is given by $\tau = R_m C_m$. Note that the time constant corresponds to a characteristic frequency (in hertz), $f^* = (2\pi R_m C_m)^{-1}$.

As described above, the presence of ion channels in a membrane provides a parallel low impedance conduction pathway. If the resistance associated with all the channels in the membrane $R_{\text{ch}} < R_{\text{bilayer}}$, then $R_m \approx R_{\text{ch}}$. Thus, the presence of a sufficient number of conducting channels in the membrane will result in a decrease in the membrane resistance and hence an increase in the time constant.

The resolution of such measurements can be determined in the following way. Recalling that $1/R_{\text{ch}} = n_{\text{ch}} g_{\text{ch}}$, we obtain $n_{\text{ch}} = 1/g_{\text{ch}} R_{\text{bilayer}}$ at the point where $R_{\text{ch}} = R_{\text{bilayer}}$. Thus, for a membrane with $R_{\text{bilayer}} = 1 \times 10^5$ Ω cm^2 and $g_{\text{ch}} = 20$ pS, we obtain a resolution for impedance measurements of 5×10^5 cm^{-2}. This is equivalent to one channel per 2×10^{-6} cm^2(200 μm^2).

A. Simulations

Figures 2 and 3 show simulations of the impedance response for the equivalent circuit shown in Fig. 1, according to Eq. (4). The impedance response is presented as the frequency dependence of the magnitude (often referred to as the Bode plot) and phase angle determined from Eqs. (5) and (6), respectively. Figure 2 shows the magnitude and frequency for $R_s = 10$ Ω, $R_{\text{ct}} = 1$ M Ω, $C_p = 10$ μF, $C_m = 1$ μF, and R_m from 10^2–10^7 Ω. The simulations demonstrate that

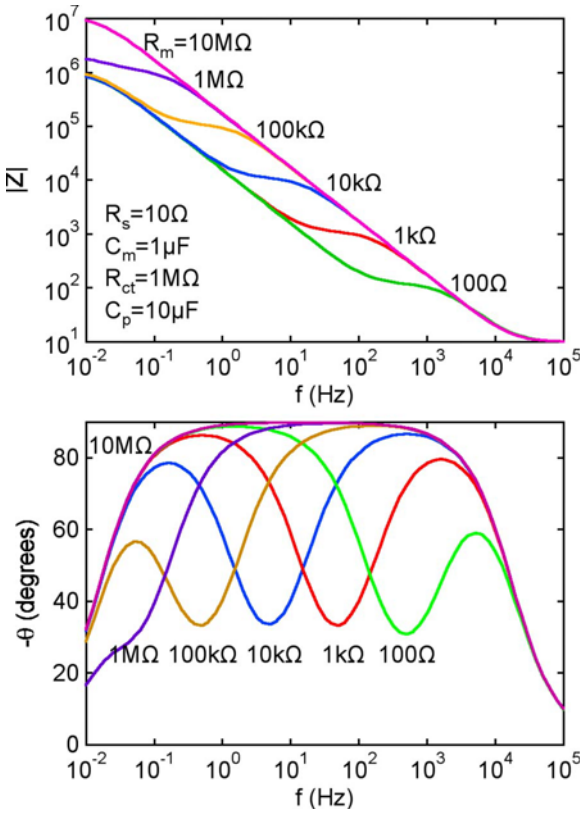

FIG. 2. Simulations of the impedance response of supported bilayers. (Top) Bode plot and (bottom) phase angle for the equivalent circuit shown in Fig. 1. Simulation parameters: $R_s=10\ \Omega$, $R_{ct}=1\ \mathrm{M}\Omega$, $C_{sc}=10\ \mu\mathrm{F}$, $C_m=1\ \mu\mathrm{F}$, and $R_m=10^2-10^7\ \Omega$. The high frequency response is due to the membrane (R_m and C_m), whereas the lower frequency response is due to the silicon support (R_{ct} and C_p). The two peaks in the phase angle plot correspond to the inverse of the time constant for the two RC networks ($R_{ct}C_p$ and R_mC_m). The inflection point in the Bode plot corresponds to the transition between the two regimes.

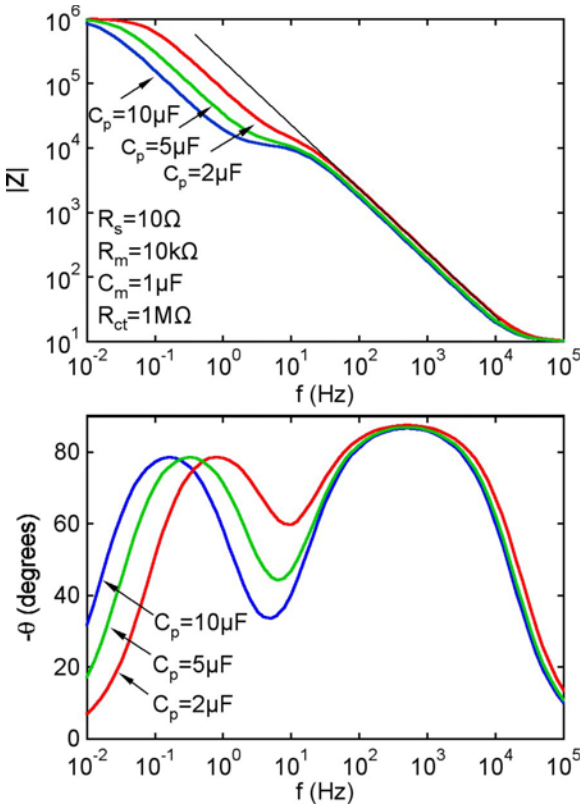

FIG. 3. Simulations of the impedance response of supported bilayers illustrating the influence of C_p. (Top) Bode plot and (bottom) phase angle for the equivalent circuit shown in Fig. 1. Simulation parameters: $R_s=10\ \Omega$, $R_{ct}=1\ \mathrm{M}\Omega$, $C_m=1\ \mu\mathrm{F}$, $R_m=10^4\ \Omega$, and $C_p=2$, 5, and 10 $\mu\mathrm{F}$. These results show that the membrane impedance can be detected as long as the minimum space charge layer of the silicon is greater than about 2 $\mu\mathrm{F\ cm^{-2}}$.

the impedance response has two contributions separated by a frequency-dependent inflection point. The higher frequency response is due to the membrane, whereas the lower frequency response is due to the silicon support. The two peaks in the phase angle plot correspond to the inverse of the time constant for the two RC networks. The transition between the two regimes on the ordinate corresponds to the sum of the series resistance R_s and the membrane resistance R_m. Thus, as long as $R_s \ll R_m$, then the y-axis intercept can be used to determine the membrane resistance.

The characteristic response of an ideal capacitor in a Bode plot is a straight line with a slope of -1. In this linear region the capacitance can be obtained from $Z_{\mathrm{imag}}=(i2\pi fC)^{-1}$, and is constant at all frequencies. Since $f^*=(2\pi R_mC_m)^{-1}$ and recalling that $C_m=1\ \mu\mathrm{F}$, the characteristic frequency shifts from 0.02 Hz for $R_m=10^7\ \Omega$ to 2×10^3 Hz for $R_m=10^2\ \Omega$.

To observe an inflection point at the transition between the two regimes, C_m must be less than C_p. Figure 3 shows the impedance response for $R_s=10\ \Omega$, $R_{ct}=1\ \mathrm{M}\ \Omega$, $C_m=1\ \mu\mathrm{F}$, $R_m=10^4\ \Omega$, and $C_p=2$, 5, and 10 $\mu\mathrm{F}$. As C_p decreases, the capacitive relaxations between the two regimes become closer and the transition region becomes smaller. However, the transition between the two regimes can be distinguished even with $C_p=2\ \mu\mathrm{F}$, i.e., for $C_p/C_m=2$.

From the simulations we can see an important requirement to allow measurement of the impedance due to ion channels. C_m should be less than C_p so that the impedance of the membrane will be greater than that of the silicon, thus allowing the C_m contribution to be distinguished. This constraint is discussed in more detail below.

B. The parallel capacitance

As described above, the parallel capacitance C_p consists of the space charge layer capacitance C_{sc} of the semiconductor in series with the double layer capacitance C_{dl} associated with the silicon/solution interface. The parallel capacitance $C_p(=C_{dl}C_{sc}/(C_{dl}+C_{sc}))$ is equal to the smaller of the two contributions. Analysis of the parallel capacitance is complicated by the fact that both terms are dependent on potential.

The space charge layer capacitance for an n-type semiconductor is potential dependent and is given by[15]

$$C_{sc} = \left(\frac{\varepsilon\varepsilon_0 e^2 N_D}{2kT}\right)^{1/2} \left|\left(\exp\left(-\frac{e(U-U_{fb})}{kT}\right)-1\right)\right| \times \left[\exp-\left(\frac{e(U-U_{fb})}{kT}\right)+\frac{e(U-U_{fb})}{kT}-1\right]^{-1/2}, \quad (7)$$

where U is the applied potential, U_{fb} is the flatband potential, ε is the relative permittivity, ε_0 is the permittivity of free space, N_D is the ionized donor concentration, e is the charge on the electron, k is the Boltzmann constant, and T is temperature.

In the depletion regime where $U-U_{fb}>3$ kT/e, Eq. (7) reduces to

$$\frac{1}{C_{sc}^2} = \left(\frac{2}{eN_D\varepsilon\varepsilon_0}\right)\left(U-U_{fb}-\frac{kT}{e}\right). \quad (8)$$

This is the Mott-Schottky relation where $U-U_{fb} \propto C_{sc}^{-2}$. Note that $U=U_{fb}$ when $1/C_{sc}^2+\mathrm{kT}/e=0$. For moderately doped semiconductors (N_D up to about 10^{18} cm^{-3}) in the depletion regime, the capacitance of the space charge layer is in the range from 10 to 100 nF cm^{-2}. However, for high dopant densities ($N_D>10^{18}$ cm^{-3}) C_{sc} may be larger than 1 μF cm^{-2}.

In the accumulation regime at sufficiently large band bending ($U-U_{fb}<-3$ kT/e), Eq. (7) reduces to

$$C_{sc} = \left(\frac{\varepsilon\varepsilon_0 e^2 N_D}{2kT}\right)^{1/2} \exp\left(-\frac{e(U-U_{fb})}{2kT}\right). \quad (9)$$

Thus, for $U-U_{fb}<0$, the space charge layer capacitance increases exponentially, and can reach values in excess of 1 μF cm^{-2} at relatively small values of $U-U_{fb}$. Since the flatband potential for silicon is typically in the range from 0 to −0.5 V (Ag/AgCl),[16] large values of the space charge layer capacitance can be achieved at potentials negative to the flatband potential, independent of the dopant density. The impedance of the semiconductor/solution interface may be further complicated by the presence of surface states or an oxide layer.[17,18]

In summary, to satisfy the condition for measuring the membrane capacitance, i.e., $C_m<C_p$, we can see that both C_{sc} and C_{dl} must be greater than the membrane capacitance, which is typically 0.5–1 μF cm^{-2}. The double layer capacitance at a semiconductor/solution interface is typically 1–10 μF cm^{-2}; hence, we must ensure that space charge capacitance $C_{sc}>1$ μF cm^{-2}. This can be achieved by using highly doped silicon (large N_D) or by performing measurements at potentials where $U<U_{fb}$.

III. MATERIALS AND EXPERIMENTAL METHODS

All experiments were performed on highly doped silicon, n^+-Si(111) (Montco Silicon Technologies, Inc., Spring City, PA) with $N_D=2\times10^{19}$ cm^{-3} or moderately doped silicon, n-Si(111) (Montco Silicon Technologies, Inc., Spring City, PA) with $N_D=1\times10^{17}$ cm^{-3}. Clean hydrophilic surfaces are required for LB deposition of uniform monolayers, and the wafers were therefore cleaned in piranha solution prior to monolayer deposition. Briefly, the wafers were immersed sequentially in 2-propanol (Fisher Scientific, Assay 99.9%), acetone (J.T. Baker, assay 99.8%), and 2-propanol, and sonicated for 15 min with each solvent. Finally, the wafers were immersed in piranha etch solution: 30% hydrogen peroxide (Fisher Scientific, Assay 95.4) and 70% sulfuric acid (Fisher Scientific, Assay 31.4%). The wafers were etched for 20 min and then rinsed several times in deionized water prior to deposition of the bilayer.

DPhPC lipid bilayers were formed by LB deposition and vesicle fusion. In the first step, Langmuir-Blodgett (LB) deposition was used to form the lower leaflet on the silicon support. The lipid, 1,2-diphytanoyl-sn-glycero-3-phosphocholine (DPhPC) and polyethylene glycol–modified lipid, 1,2-dipalmitoyl-sn-glycero-3-phosphoethanolamine-*N*-[methoxy(polyethylene glycol)-2000] (PEG-2k) were purchased from Avanti Polar Lipids (Alabaster, AL) and used without further purification. Lipids were premixed in chloroform to achieve a total concentration of 1 mg mL^{-1}. The concentration of PEG-2k was 5.9 mol % based on the total lipid concentration. This concentration is the estimated crossover concentration for the PEG polymer chain (i.e., the transition from the "mushroom" to the "brush" regime) and corresponds to the concentration where the random PEG coils begin to come into contact with each other. A lipid monolayer was deposited on a silicon substrate from a Langmuir trough (model 611D, Nima Technology Ltd., Coventry, England). A clean silicon wafer was attached to the motor driven stage and submerged in the subphase, 18 MΩ cm water (Milli-Q, Millipore, Bedford, MA). Next, 25 μL of the lipid solution was spread dropwise at the air-water interface of the open trough (600 cm^2). After spreading, the chloroform was allowed to evaporate for 15 min and then the monolayer was compressed at a barrier speed of 100 cm^2 min^{-1} to a pressure of 32 mN m^{-1}. The silicon substrates were withdrawn from the trough at 15 mm min^{-1} while maintaining the pressure constant at 32 mN m^{-1}. This rate was sufficiently slow to ensure that the meniscus formed at the silicon surface remained uniform during withdrawal.

After LB deposition of the monolayer, the silicon wafer was assembled into a three-electrode electrochemical cell. An ohmic contact was formed on the wafer using InGa eutectic after surface oxide removal by a careful application of 25% HF for 1 min. The bilayer was then completed by vesicle fusion (VF) of large unilamellar vesicles (LUVs). Large LUVs were prepared using standard techniques; the details have been reported elsewhere.[14] A solution of 0.5 mL of the vesicles was slowly introduced into the electrochemical cell using a pipette. The bilayers were completed by incubation of the vesicles in the dark for 1 hour. Prior to electrochemical measurements, additional PBS was added to a total volume of about 8 mL. All experiments were performed in 100 mM potassium phosphate buffer (sodium phosphate dibasic $Na_2HPO_4.7H_2O$, 98–100%, J. T. Baker, NJ, and sodium phosphate monobasic NaH_2PO_4, 100%, J. T. Baker, NJ) with 100 mM KCl (99.4%, J. T. Baker, NJ), *p*H 6.9–7.1. The cell included a Ag/AgCl (3 M NaCl) reference electrode and a platinum mesh counter electrode. All potentials are reported with respect to the Ag/AgCl reference (U_{eq}

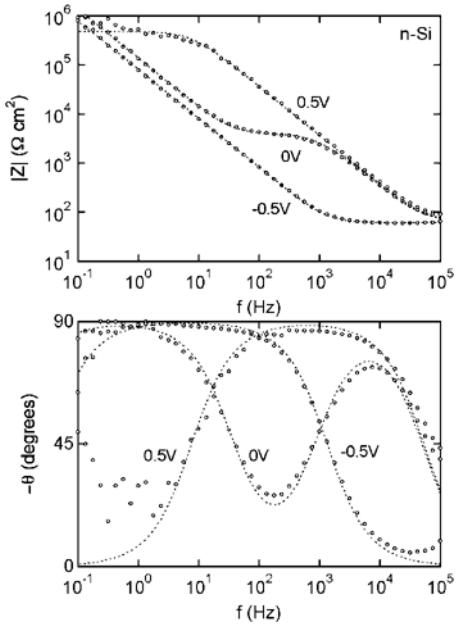

FIG. 4. (Top) Magnitude and (bottom) phase angle of the impedance for *n*-Si(111) in PBS at −0.5, 0, and 0.5 V (Ag/AgCl). The dotted lines show the nonlinear least-squares fits to the spectra.

=0.200 V vs SHE). Impedance measurements were performed with a 20 mV rms ac perturbation over the frequency range from 0.1 Hz to 100 kHz. All experiments were conducted in the dark, to avoid photoeffects in the silicon, and at room temperature.

IV. RESULTS AND DISCUSSION

A. *n*-Si

The magnitude and phase angle of the impedance for *n*-Si in PBS at three different potentials is shown in Fig. 4. The dotted lines correspond to nonlinear least-squares fits using a resistance (R_s) in series with a single parallel *RC* network (R_{ct} and C_p) from which we can extract the values of R_s, R_{ct}, and C_p. At +0.5 and −0.5 V a single capacitive relaxation is seen, corresponding to the parallel capacitance C_p in the equivalent circuit. The magnitude of the impedance at +0.5 V is almost two orders of magnitude larger than the impedance at −0.5 V, implying that the capacitance at +0.5 V is about two orders of magnitude smaller. The slope in the linear region is very close to −1.0, characteristic of a near-ideal capacitor. This can also been seen in the phase angle where the maximum is close to 90°. However, over a range of potentials from 0.4 to −0.2 V, two capacitive relaxations are observed (see the spectrum at 0 V in Fig. 4). In this potential range the equivalent circuit is more complicated than the circuit shown in Fig. 1.

Figure 5 shows the capacitance for *n*-Si in PBS. At positive potentials, in the depletion regime, the capacitance is 40−80 nF cm^{-2}, characteristic of the silicon space charge layer capacitance. At more negative potentials a second contribution due to the silicon/solution interface is seen that

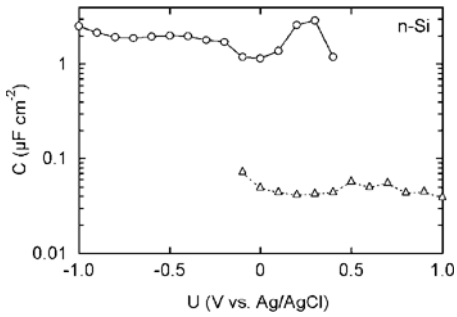

FIG. 5. Measured parallel capacitance (C_p) vs potential for *n*-Si(111) in PBS. (*o*) capacitive relaxation due to the silicon/solution interface, and (Δ) capacitive relaxation due to the silicon space charge layer. Both capacitive contributions coexist in the potential range from 0.4 to −0.2 V (see Fig. 4).

dominates at potentials more negative than −0.2 V. Both capacitive contributions are observed in the potential range from 0.4 to −0.2 V, as can be seen from the impedance spectrum at 0 V in Fig. 4. The capacitance in this regime is about 2 μF cm^{-2}, slightly larger than a typical membrane capacitance. Thus, the parallel capacitance C_p is only slightly larger than the typical bilayer membrane capacitance over a range of potentials from −0.3 to −1.0 V.

For an *n*-type semiconductor in a solution, the depletion of majority carriers occurs at potentials positive to the flatband potential. In the depletion regime the space charge layer capacitance is very small, typically less than 100 nF cm^{-2}. Note that the capacitance due to the silicon (Fig. 5) does not show good agreement with the Mott-Schottky relation [Eq. (9)] due to the presence of the thin oxide layer in the buffer solution. At more negative potentials, the space charge layer capacitance increases and, at −0.3 V, only the double layer capacitance is observed. Thus, the potential range that satisfies the condition $C_m < C_p$, assuming a membrane capacitance of about 1 μF cm^{-2}, is from −0.3 to −1.0 V.

B. *n*-Si/DPhPC

Figure 6 shows the magnitude and phase angle for *n*-Si with a DPhPC bilayer at +0.5 and −0.5 V. The bilayer was formed by LB deposition of DPhPC and 5.9 mol % PEG2k at 32 mN m^{-1}, followed by fusion of DPhPC vesicles, as described in Sec. III. The lower leaflet includes a fraction of lipids with a polyethylene glycol group attached to the head group, providing a polymer cushion, or spacer layer, isolating the bilayer from the solid support. The dotted lines correspond to nonlinear least-squares fits using the equivalent circuit shown in Fig. 1 from which we can extract the values of R_s, R_m, C_m, R_{ct}, and C_p.

At +0.5 V the impedance is large due to the small capacitance of the silicon space charge layer. At −0.5 V the parallel capacitance is dominated by the double layer and hence the impedance of the membrane can be resolved over the frequency range from about 10 Hz to 10 kHz. Comparison to the impedance of *n*-Si in PBS at the same potential (Fig. 4), clearly reveals the additional contribution to the impedance. The transition between the relaxations is evident by the in-

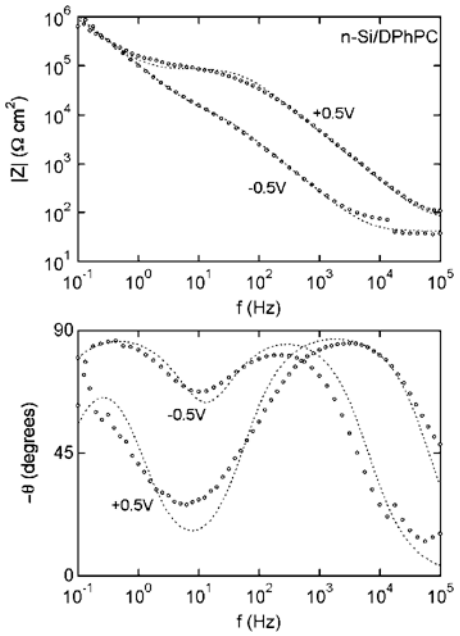

FIG. 6. (Top) Magnitude and (bottom) phase angle of the impedance for a DPhPC bilayer on *n*-Si(111) in PBS at −0.5 and +0.5 V (Ag/AgCl). The Bode plot shows two relaxations: the higher frequency response is due to the bilayer (C_m) and the lower frequency response is due to the silicon/solution interface (C_p). The dotted lines show the nonlinear least-squares fits to the spectra.

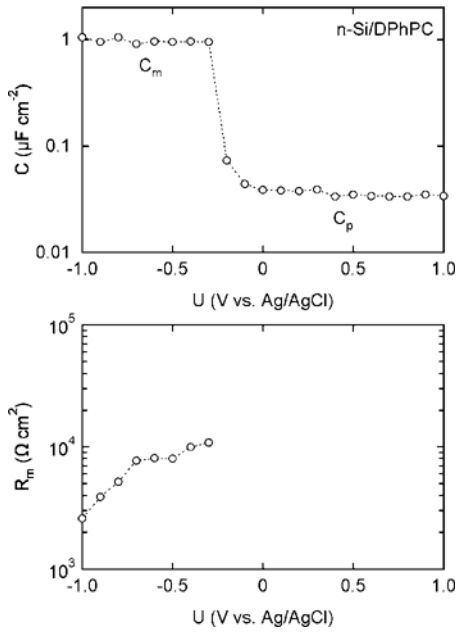

FIG. 7. (Top) Capacitance vs potential for a DPhPC bilayer on *n*-Si(111) in PBS. At potentials from −0.3 to −1.0 V, the membrane capacitance is measured since $C_m < C_p$. At more positive potentials, $C_p < C_m$ and the silicon space charge layer capacitance is measured. (Bottom) Bilayer resistance vs potential obtained from nonlinear least-squares fits of the impedance spectra at each potential.

flection point at about 2 Hz ($10^4\ \Omega\ \mathrm{cm}^2$). The contribution of the membrane can also be seen from the frequency dependence of the phase angle at −0.5 V, where the two peaks correspond to the two time constants at about 2 and 200 Hz. Comparison to Fig. 4 shows that the phase angle for *n*-Si in PBS at −0.5 V shows a single time constant. Also note that the least-squares fit for the spectrum at +0.5 V, where the impedance is dominated by the silicon space charge layer, is not as good as at −0.5 V, where the membrane impedance is measured.

The capacitance of a DPhPC membrane on *n*-Si is shown in Fig. 7. As expected,the membrane capacitance of about $1\ \mu\mathrm{F\ cm}^{-2}$ is only measured over the potential range from −0.3 to −1.0 V where $C_m < C_p$. At potentials positive to −0.3 V, the measured capacitance decreases dramatically as the parallel capacitance is dominated by the space charge layer capacitance since $C_p < C_m$. The corresponding values of the membrane resistance, also shown in Fig. 7, increase from $3\times10^3\ \Omega\ \mathrm{cm}^2$ at −1.0 V to about $1\times10^4\ \Omega\ \mathrm{cm}^2$ at −0.3 V. These results demonstrate that membrane measurements can be made on low or moderately doped silicon over a narrow potential range. This is the potential range where the silicon is in weak depletion or accumulation such that $C_m < C_p$. The dependence on applied potential suggests that the membrane resistance is dependent on the magnitude and sign of the electric field across the membrane. A similar effect is seen over a much wider potential range for bilayers formed on n^+-Si (see below).

The condition that $C_m < C_p$ is essential for measuring the impedance of bilayer membranes. In the simplest case, as discussed here, C_p has two components, the space charge layer capacitance of the semiconductor and the double layer capacitance at the interface. The space charge layer capacitance is strongly dependent on potential, as described above. In most cases where the ionic strength of the solution is sufficiently large, the double layer capacitance can be modeled as a parallel plate capacitor, according to the Helmholtz model. The double layer capacitance for most semiconductors is $1-10\ \mu\mathrm{F\ cm}^{-2}$ and only weakly dependent on potential, consistent with the Helmholtz model.[15] Since C_p is dependent on applied bias, it is crucial to understand this potential dependence in making measurements on bilayer membranes.[14,19]

C. n^+-Si

Figure 8 shows the magnitude and phase angle for n^+-Si in PBS. Over the potential range of interest from −1 to +1 V, the impedance response exhibits a single capacitive relaxation. The phase angle reaches a maximum value close to 90° characteristic of an ideal capacitor. The dotted lines show the least-squares fit to the spectrum using a resistance (R_s) in series with a single parallel *RC* network (R_{ct} and C_p). Figure 9 shows that the parallel capacitance C_p increases from about $2\ \mu\mathrm{F\ cm}^{-2}$ at +1.0 V to about $3\ \mu\mathrm{F\ cm}^{-2}$ at −1.0 V. These values are relatively large across the whole potential range due to the high donor density of the silicon. Thus, the parallel capacitance C_p is larger than the typical bilayer membrane capacitance of about $1\ \mu\mathrm{F\ cm}^{-2}$ over a wide potential range, satisfying the condition that $C_m < C_p$.

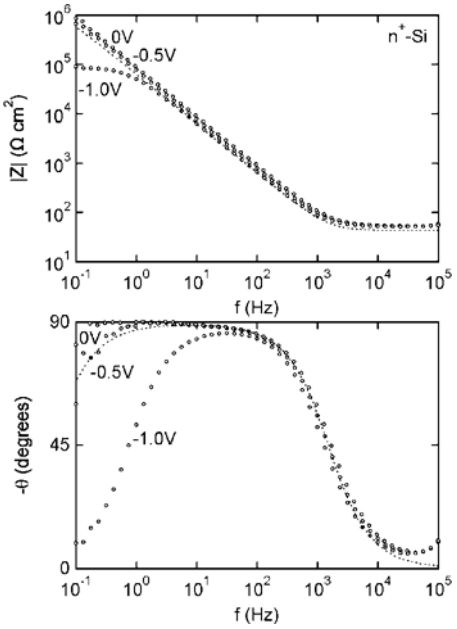

FIG. 8. (Top) Magnitude and (bottom) phase angle of the impedance for n^+-Si(111) in PBS at −1.0, −0.5, and 0 V (Ag/AgCl). The Bode plot shows a single capacitive relaxation (C_p) with a phase angle very close to −90°, corresponding to an ideal parallel plate capacitor. The dotted line shows the nonlinear least-squares fit for the spectrum at −0.5 V.

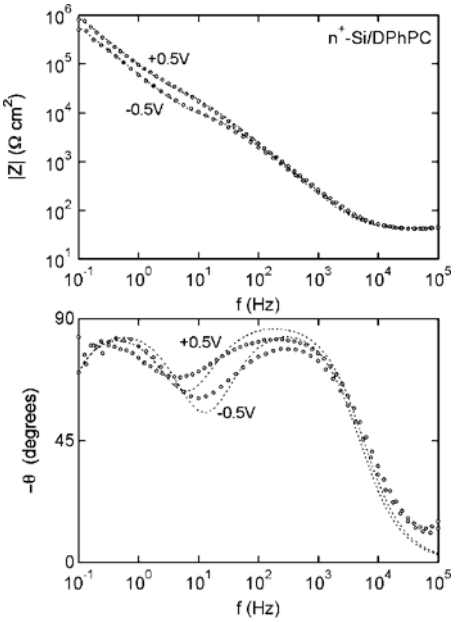

FIG. 10. (Top) Magnitude and (bottom) phase angle of the impedance for DPhPC bilayers on n^+-Si(111) in PBS at −0.5 and +0.5 V (Ag/AgCl). The Bode plot shows two relaxations: the higher frequency response is due to the bilayer (C_m) and the lower frequency response is due to the silicon/solution interface (C_p).

D. n^+-Si/DPhPC

The magnitude and phase angle of the impedance of a DPhPC bilayer on n^+-Si at two potentials is shown in Fig. 10. The Bode plots at −0.5 and +0.5 V both show the characteristic features of a series combination of two parallel *RC* networks. The higher frequency relaxation is associated with the bilayer and the lower frequency relaxation is associated with the parallel capacitance. The dotted lines correspond to the nonlinear least-squares fits to the spectra using the equivalent circuit shown in Fig. 1, from which we can obtain the values of the circuit elements.

Figure 11 shows the bilayer capacitance obtained from analysis of the high frequency part of the impedance spectra. The capacitance is about 1 μF cm^{-2} over the measured potential range from +1 to −1 V. This result indicates that the bilayer is stable over a wide potential range. The membrane resistance, also shown in Fig. 11, increases from about 7×10^3 Ω cm^2 at −1 V to about 4×10^4 Ω cm^2 at +1 V. The values for the bilayer resistance are very similar to the values

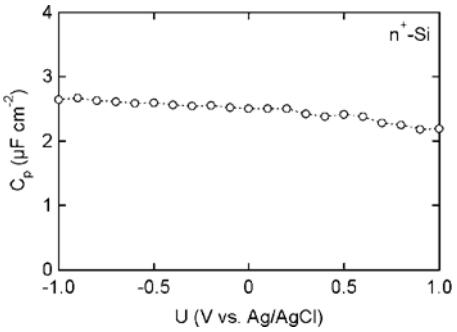

FIG. 9. Parallel capacitance (C_p) vs potential for n^+-Si(111) in PBS. The capacitance was obtained from nonlinear least-squares fits to the spectra using an equivalent circuit consisting of a resistance R_s in series with a single parallel *RC* loop (R_{ct} and C_p).

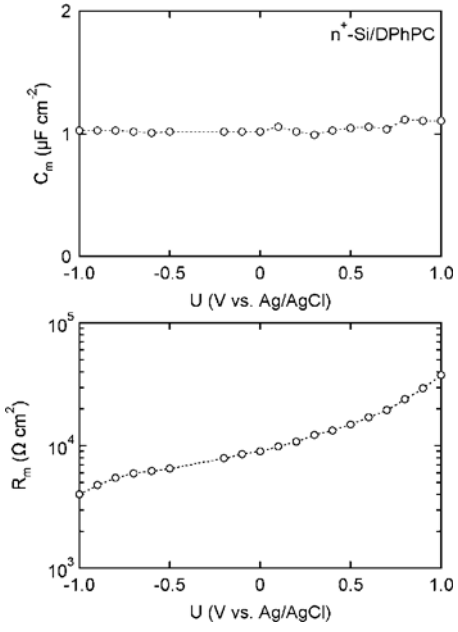

FIG. 11. (Top) Bilayer capacitance, (middle) bilayer resistance, and (bottom) bilayer admittance vs potential for a DPhPC bilayer on n^+-Si(111) in PBS. Both C_m and R_m were obtained from nonlinear least-squares fits to the spectra using an equivalent circuit shown in Fig. 1.

measured on *n*-Si in the potential range from −0.3 to −1.0 V, where R_m could be measured. The increase in membrane resistance with increasing potential is unexpected and suggests that the resistance is dependent on the magnitude and sign of the electric field across the membrane.

V. SUMMARY

The integration of bilayer membranes with semiconductors provides the potential for hybrid bioelectronic devices and structures. In integrating bilayers with semiconductor supports, a detailed understanding of the electrical properties of the semiconductor/solution interface is critical in determining appropriate regimes for measuring the electrical properties of the bilayer and for further studies in detecting signal transduction through a bilayer by means of transmembrane proteins. Here, we demonstrate that highly doped *n*-Si provides a wide potential range for electrical measurements of bilayer membranes.

[1]E. Sackmann, Science **271**, 43 (1996).
[2]H. Lang, C. Duschl, and H. Vogel, Langmuir **10**, 197 (1994).
[3]B. Raguse, V. Braach-Maksvytis, B. A. Cornell, L. G. King, P. D. J. Osman, R. J. Pace, and L. Wieczorek, Langmuir **14**, 648 (1998).
[4]R. Naumann, S. M. Schiller, F. Giess, B. Grohe, K. B. Hartman, I. Karcher, I. Koper, J. Lubben, K. Vasilev, and W. Knoll, Langmuir **19**, 5435 (2003).
[5]F. Giess, M. G. Friedrich, J. Heberle, R. L. Naumann, and W. Knoll, Biophys. J. **87**, 3213 (2004).
[6]S. Lingler, I. Rubinstein, W. Knoll, and A. Offenhausser, Langmuir **13**, 7085 (1997).
[7]M. L. Wagner and L. K. Tamm, Biophys. J. **79**, 1400 (2000).
[8]V. Kiessling and L. K. Tamm, Biophys. J. **84**, 408 (2003).
[9]C. Steinem, A. Janshoff, W. P. Ulrich, M. Sieber, and H. J. Galla, Biochim. Biophys. Acta - Biomembranes **1279**, 169 (1996).
[10]S. Gritsch, P. Nollert, F. Jahnig, and E. Sackmann, Langmuir **14**, 3118 (1998).
[11]P. Fromherz, V. Kiessling, K. Kottig, and G. Zeck, Appl. Phys. A: Mater. Sci. Process. **69**, 571 (1999).
[12]O. Purrucker, H. Hillebrandt, K. Adlkofer, and M. Tanaka, Electrochim. Acta **47**, 791 (2001).
[13]V. Atanasov, N. Knorr, R. S. Duran, S. Ingebrandt, A. Offenhausser, W. Knoll, and I. Koper, Biophys. J. **89**, 1780 (2005).
[14]V. Nikolov, J. Lin, M. Merzlyakov, K. Hristova, and P. C. Searson, Langmuir **23**, 13040 (2007).
[15]A. Natarajan, G. Oskam, and P. C. Searson, J. Phys. Chem. B **102**, 7793 (1998).
[16]S. R. Morrison, *Electrochemistry at Semiconductor and Oxidized Metal Electrodes* (Plenum, New York, 1980), p. xiv.
[17]G. Oskam, J. C. Schmidt, P. M. Hoffmann, and P. C. Searson, J. Electrochem. Soc. **143**, 2531 (1996).*n*
[18]P. M. Hoffmann, G. Oskam, and P. C. Searson, J. Appl. Phys. **83**, 4309 (1998).
[19]V. Nikolov, A. Radisic, K. Hristova, and P. C. Searson, Langmuir **22**, 7156 (2006).